

Raman scattering and infrared reflectivity study of orthorhombic/monoclinic LaTiNbO₆ microwave dielectric ceramics by A/B-site substitution

Jian Zhang, Ruzhong Zuo*

Institute of Electro Ceramics & Devices, School of Materials Science and Engineering, Hefei University of Technology, Hefei 230009, PR China



ARTICLE INFO

Keywords:
Ceramics
Dielectric response
Vibrational spectroscopy
Aeschnynite

ABSTRACT

The structure origin of microwave dielectric properties in A/B-site substituted LaTiNbO₆ ceramics with different crystal structures was explored by means of Raman scattering and infrared reflection spectra. Compared with the monoclinic (M) phase, the broadening of the Raman modes associated with B–O stretching and bending vibrations in the orthorhombic (O) phase was believed to be a result of the increased octahedral distortion. The Raman mode at 659 cm⁻¹ was assigned to the stretching vibration of B–O–B and O–B–O bonds in the unique interlayer chain structure of O phase. The Raman modes of the BO₆ tilting within 340–520 cm⁻¹ suggest that different octahedral connection ways should be one of the vital reasons why M and O phases own opposite-sign temperature coefficient of resonance frequency τ_f . Moreover, the result of infrared reflection spectrum fitted with a four-parameter semiquantum model indicates that the dielectric response of both M and O phases would mainly originate from the A-BO₆ external vibrations in the far-infrared frequency, particularly their AO₈ structure units. These results would provide useful insights into the structure-property relation in the RETi(Nb,Ta)O₆ (RE: rare earth) material system.

1. Introduction

A family of RETi(Nb,Ta)O₆ (RE: rare-earth ions) materials with general formula AB₂O₆ has shown great potentials in a variety of fields, such as mobile and satellite communication systems, miniature solid-state laser, and luminescence applications [1–6]. LaTi(Nb,Ta)O₆ belongs to a special one in this family. It crystallizes in an orthorhombic (O) aeschnynite structure with *Pnma* space group at low temperatures, but transforms into a high-temperature monoclinic (M) aeschnynite structure with *C2/c* space group [7]. For LaTiNbO₆ ceramics, the high-temperature M phase could stably exist at room temperature, having microwave dielectric properties of permittivity $\epsilon_r \sim 22.3$, quality factor $Q \times f \sim 49867$ GHz and temperature coefficient of resonance frequency $\tau_f \sim -55$ ppm/°C [8]. By comparison, it is rather difficult to attain a single O-phase ceramic only if some special measures are taken [9,10]. A dense O-phase ceramic was reported to own microwave dielectric properties of $\epsilon_r \sim 63$, $Q \times f \sim 9600$ GHz (@4.77 GHz) and $\tau_f \sim 105$ ppm/°C [10]. It can be found that the former aeschnynite has a negative τ_f and a low ϵ_r , while the latter one presents a positive τ_f and a relatively high ϵ_r . In addition, the A/B-site substitution was found to effectively control the M–O phase transition of LaTiNbO₆ matrix,

leading to a few superior composite ceramics with a near-zero τ_f value [11,12]. Experimental results have indicated an obvious correlation between the decrease of octahedral distortion and the instability of M phase in LaTiNbO₆ ceramics.

Nevertheless, there are still rare reports on the origin of dielectric responses in such a special structure. Vibrational spectroscopy has been successfully used to probe structural features, crystal chemistry, and phase transitions in a variety of electroceramics [13–17]. For instance, the variation of local structure during the phase evolution of (1-x)BiVO₄-xLaNbO₄ ceramics was revealed by Raman spectroscopy [13]. The infrared spectroscopy was used to disclose the vibration modes of the most remarkable dielectric contribution in CeVO₄-TiO₂ microwave dielectric ceramics [14]. These techniques have been also effectively combined in many complex perovskites to investigate the behavior of the polar phonon modes, which represents the intrinsic dielectric contributions and the local crystalline structure [15–17].

In this work, the local structure of A/B-site substituted LaTiNbO₆ ceramics was specially analyzed by means of Raman scattering and infrared reflection spectroscopy. A special focus was on exploring the structure origin of distinct microwave dielectric properties among LaTiNbO₆ ceramics with different phase structures.

* Corresponding author.

E-mail address: piezolib@hfut.edu.cn (R. Zuo).

<https://doi.org/10.1016/j.ceramint.2018.05.194>

Received 21 February 2018; Received in revised form 5 May 2018; Accepted 22 May 2018
Available online 23 May 2018

0272-8842/© 2018 Elsevier Ltd and Techna Group S.r.l. All rights reserved.

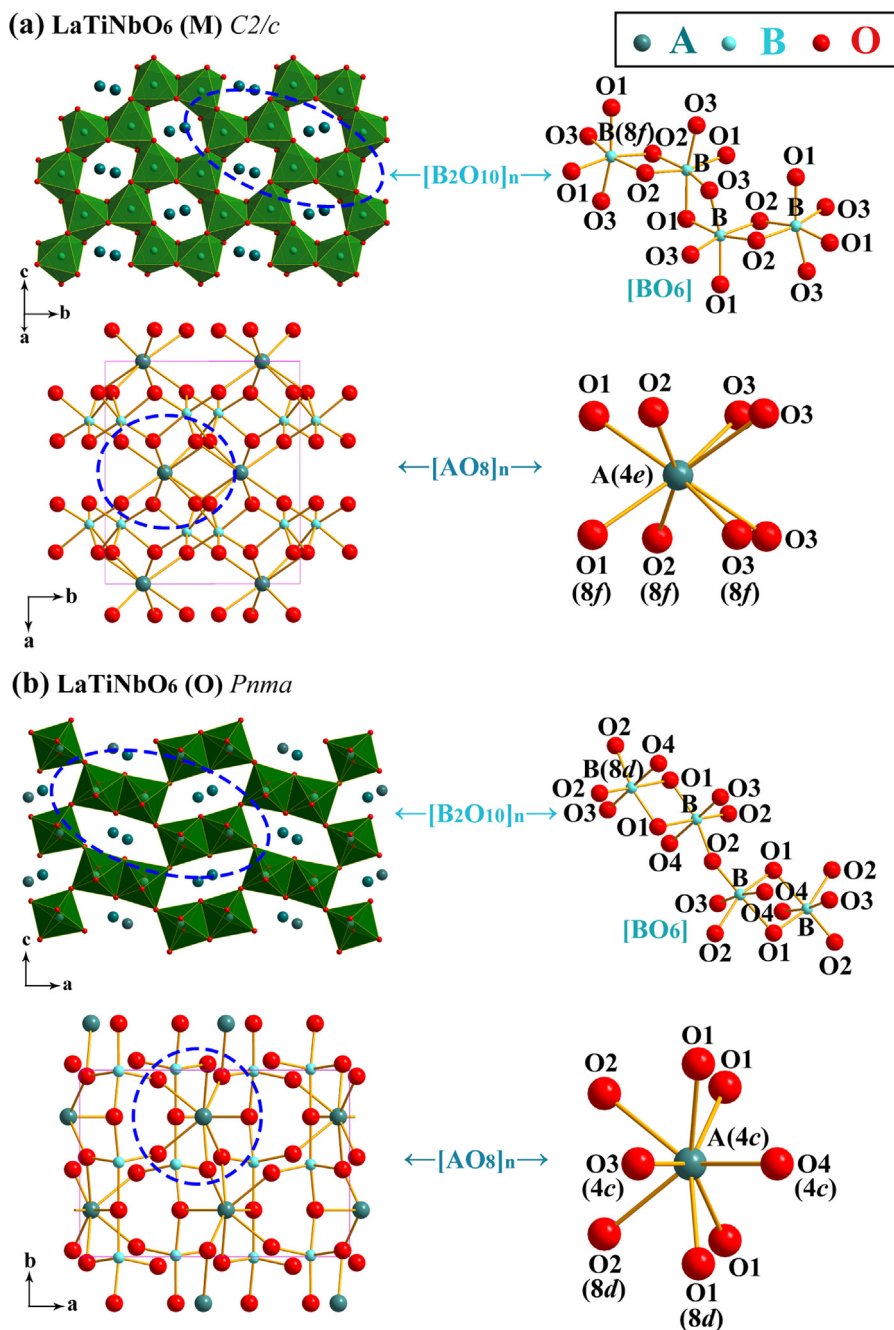


Fig. 1. Schematic diagrams of the crystal structure in (a) M- and (b) O-phase LaTiNbO_6 together with sphere-rod graphs of the B_2O_{10} (including BO_6 unit) and AO_8 polyhedron.

2. Experimental procedure

Ceramics in this work were prepared by a routine solid-state reaction process, as described in Refs. [9,11,12] where their microwave dielectric properties were reported by means of a network analyzer (Agilent, N5230C, Palo Alto, CA). The signs of M, M-A and M-B stand for the LaTiNbO_6 ceramics with non-doping [9], 5 mol% Ce for the A-site La [11], and 20 mol% Ta for the B-site Nb [12], respectively. The signs of O, O-A and O-B represent the LaTiNbO_6 ceramics with non-doping [9], 20 mol% Sm for the A-site La [11], and 20 mol% Zr for the B-site Ti [12], respectively. The samples were first polished by sandpapers with different particle sizes, and then mirror-polished with a diamond abrasive (W1-W0.5) before the spectroscopy measurement. Raman spectra were collected at room temperature using a Raman

spectrometer (532 nm, LabRAM HR800, HJY, Longjumeau Cedex, France). Room-temperature infrared reflectivity spectra were measured by using a Bruker IFS 66 v FTIR spectrometer (IFS 66 v/S Vacuum; Bruker Optik GmbH, Germany) on Infrared beamline station (U4) at the National Synchrotron Radiation Laboratory (NSRL), Hefei, China.

3. Results

3.1. Group theory analysis and crystal structure characteristics

The M-phase LaTiNbO_6 exhibits the same structure as ThTi_2O_6 , belonging to $C2/c$ (C_{2h}^6) space group [18]. According to group theory described at the Bilbao Crystallographic Center website (<http://www.cryst.ehu.es/>) [19], the corresponding mode distribution of the M-

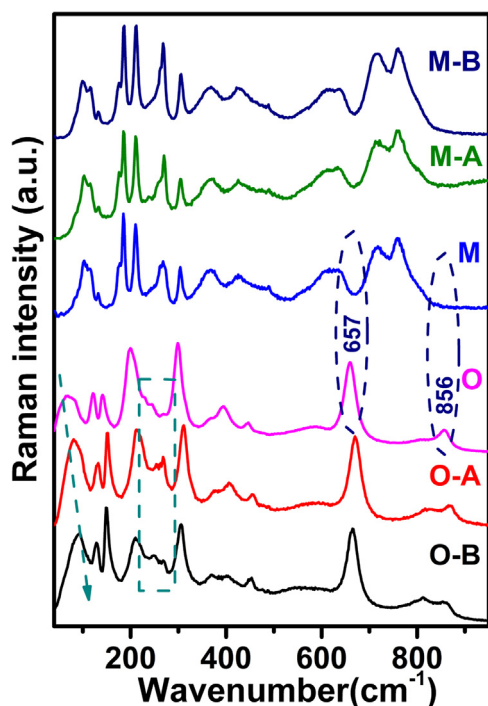


Fig. 2. Raman spectra of A/B-site substituted LaTiNbO_6 ceramics with O and M structures.

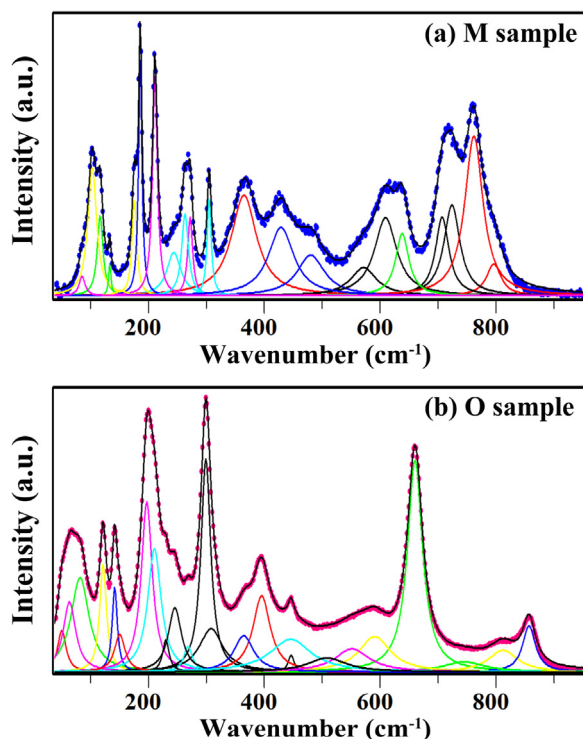
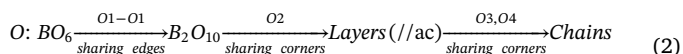


Fig. 3. Fitting curves of Raman spectra for the (a) M and (b) O samples.

phase LaTiNbO_6 can be calculated as: Au + 2Bu (acoustic), 13Ag + 14Bg (Raman) and 12Au + 12Bu (infrared). Therefore, up to 27 and 24 optical modes are expected in the Raman and infrared spectra of the M-phase LaTiNbO_6 , respectively. Moreover, the O-phase LaTiNbO_6 exhibits the same structure as CaTa_2O_6 , belonging to $Pnma$ (D_{2h}^{16}) space group [20]. Its mode distribution can be also obtained as: B1u + B2u + B3u (acoustic), 15Ag + 12B1g + 15B2g + 12B3g (Raman) and 14B1u + 11B2u + 14B3u (infrared) and 12Au (silent). As a result, up

to 54 and 39 optical modes are expected in the Raman and infrared spectra of the O-phase LaTiNbO_6 , respectively.

The schematic diagrams of the crystal structure in M- and O-phase LaTiNbO_6 are shown in Fig. 1. In both phases, a pair of BO_6 octahedra share edges to become the double-octahedron structure units B_2O_{10} , and then these units connect in different ways to form layers together with A ions located between layers. A simple structure assembly process of these two phases was summarized as follows:



In M phase, these dioctahedra B_2O_{10} form layers paralleling to bc plane through the edges O1-O3, and then these layers are parallelly stacked along a axis with A ions located between layers. However, these dioctahedra form layers paralleling to ac plane through the corners O2 in O phase, and then these layers are connected by sharing the corners O3 and O4 along b axis to form zigzag chains together with A ions located in the octahedral array gaps. In addition, the AO_8 polyhedron is also an important structure unit reflecting the connecting ways between B_2O_{10} layers, as magnified sphere-rod graphs in Fig. 1.

3.2. Raman spectra study

Fig. 2 shows the Raman spectra of the M-phase and O-phase LaTiNbO_6 ceramics with A/B-site substitution. To further study the phonon frequency and damping of each mode, the initial values of position and width were given by combining the Raman line and related literature of similar structure [21,22], and then, peak fitting was carried out by LabSpec software with Lorentz function, as representatively shown in Fig. 3. The characteristic parameters (position/width) and corresponding assignments of each mode are listed in Table 1. It can be found that the number of the observed modes is smaller than that of the predicted ones, because that some bands are too weak to be observed and other relatively weak ones are obscured by the broadening bands due to the B-site ion occupational disorder and octahedral distortion. Nevertheless, four regions with specific modes can be separated, as listed in Table 1. Particularly, the bands with wavenumbers from 170 to 340 cm^{-1} should correspond to the torque action including the double octahedral distortion or inter-chain deformation, which is primarily related with the O-B-O bending vibration.

A significant difference in the Raman spectra of M and O-phase samples can be observed from Figs. 2 and 3. A few similarities at certain bands may primarily result from their similar dioctahedron units with different connecting ways. The modes with wavenumbers of 659 cm^{-1} , 856 cm^{-1} and below 90 cm^{-1} in the O-phase sample are absent in the M-phase sample. The band at 659 cm^{-1} corresponds to the oxygen-bridged bond or the stretching vibration of B-O-B and O-B-O bonds in chains [23]. It actually reflects the interlayer connection, which should be a unique structure feature of the O phase. Besides, the bands of $< 90 \text{ cm}^{-1}$ are related to the translation and rotation of the molecule, and the band at 856 cm^{-1} corresponds to the stretching vibration of the B-O bond outside of $[\text{B}_2\text{O}_{10}]_n$ plane [24].

It can be found from Table 1 that the frequency and damping of each vibration mode are almost identical in M, M-A and M-B samples, in addition to the similarity of their spectra profiles (Fig. 2). Although the Raman spectra of three O-phase samples also look similar, yet the spectra of both O-A and O-B samples shift toward higher wavenumbers relative to that of the O sample. The blue shift in the O-A sample is larger than that in the O-B sample, indicating that the vibration of each mode in the O-A sample would need higher energy [25]. Additionally, the frequency and damping of the corresponding mode in three different O-phase samples are apparently different in the wavenumber range of $200\text{--}300 \text{ cm}^{-1}$. The vibration spectrum of the O-B sample

Table 1
Raman active modes (wavenumber/damping, in cm^{-1}) of A/B-site substituted LaTiNbO_6 ceramic pellets.

Band #	M phase			O phase			Mode assignment in LaTiNbO_6 system
	M	M-A	M-B	O	O-A	O-B	
1	85/12	86/12	91/13	50/18	65/15	60/16	60–170 cm^{-1} , La-O vibration modes
2	103/18	102/16	101/16	63/26	78/20	77/26	
3	116/12	116/14	116/14	82/38	94/28	93/27	
4	133/5	133/7	133/7	–	–	111/26	
5	152/25	149/28	153/29	121/14	131/16	129/14	
6	–	–	–	141/11	151/8	150/8	
7	–	–	–	150/22	159/19	159/24	170–340 cm^{-1} , BO_6 bending modes
8	175/10	175/12	174/12	197/23	–	–	
9	185/7	186/7	186/8	210/28	215/34	211/42	
10	211/10	211/11	211/10	230/13	–	–	
11	243/30	237/25	244/36	245/28	256/42	250/43	
12	263/14	259/20	262/14	268/18	269/9	270/10	
13	271/10	271/7	269/7	299/20	311/22	305/20	340–520 cm^{-1} , BO_6 tilting modes
14	304/8	305/10	306/10	308/49	–	311/91	
15	364/53	365/57	364/65	364/41	377/61	368/35	
16	428/53	429/50	429/52	395/36	410/41	405/72	
17	480/58	480/62	478/74	445/87	455/27	451/20	
18	–	–	–	446/12	484/23	480/63	
19	–	–	–	508/81	522/91	–	520–880 cm^{-1} , BO_6 stretching modes
20	571/55	565/38	572/70	551/72	569/71	542/93	
21	609/47	595/35	611/50	590/67	607/68	600/91	
22	637/28	615/30	640/26	659/32	670/29	665/30	
23	706/28	637/24	705/29	744/87	–	734/66	
24	723/34	716/43	722/35	–	–	782/53	
25	761/38	761/35	762/41	811/60	817/40	815/47	
26	795/31	784/25	795/39	–	839/91	–	
27	–	804/18	–	856/27	869/19	857/31	

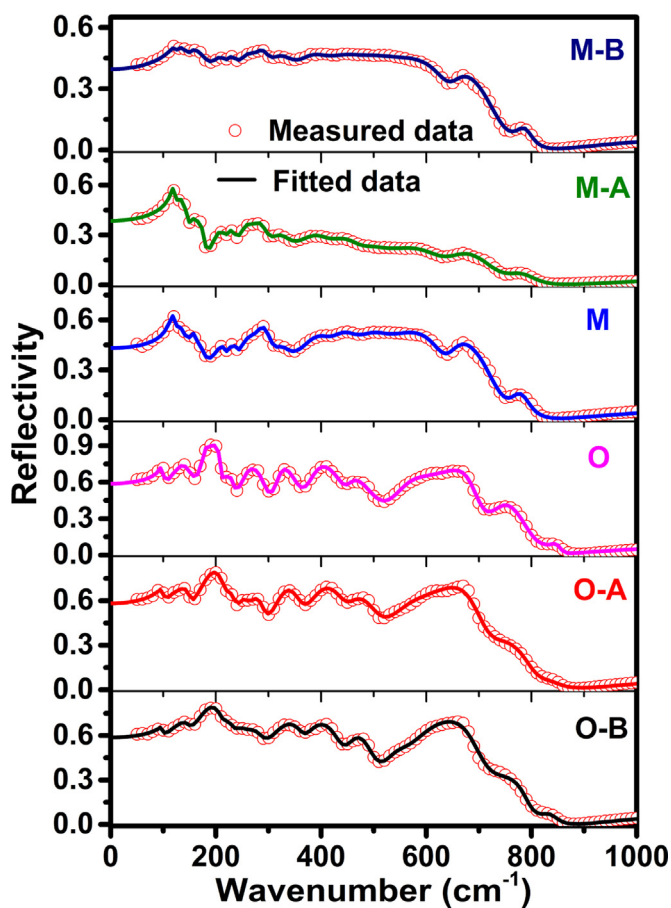


Fig. 4. Fitted and measured infrared reflectivity spectra of A/B-site substituted LaTiNbO_6 ceramics with two different structures.

becomes slightly widened during the above wavenumber range, however while the spectrum of the O-A sample becomes sharper with decreased damping, such as the mode at 269 cm^{-1} . Generally, the increased octahedral distortion should correspond to the broadening of the modes associated with B-O stretching and bending vibrations. This is consistent with the variation of the octahedral distortion observed previously [12].

3.3. Infrared reflection spectroscopy study

In order to explore the intrinsic dielectric response of a dielectric, infrared reflection spectra need to be analyzed by using the four-parameter semiquantum model (4-P) [15,26–28] with a nonlinear least-squares program [29]. According to this model, the infrared phonon contribution to the complex dielectric function $\epsilon(\omega)$ is given by

$$\epsilon(\omega) = \epsilon_\infty \prod_{j=1}^N \frac{\Omega_{j,LO}^2 - \omega^2 + i\omega\gamma_{j,LO}}{\Omega_{j,TO}^2 - \omega^2 + i\omega\gamma_{j,TO}} \tag{3}$$

where ϵ_∞ is the dielectric constant due to the electronic polarization contribution, $\Omega_{j,LO}$ ($\Omega_{j,TO}$) and $\gamma_{j,LO}$ ($\gamma_{j,TO}$) are the frequency and damping of the j th longitudinal (transverse) optical modes, respectively, and N is the number of polar phonons. At quasinormal incidence, the dielectric function is related to the optical reflectivity R by the Fresnel formula as follows:

$$R(\omega) = \left| \frac{1 - \sqrt{\epsilon(\omega)}}{1 + \sqrt{\epsilon(\omega)}} \right|^2 \tag{4}$$

Therefore, the infrared reflection spectra of the O-phase and M-phase samples can be fitted by using Eqs. (3) and (4), as shown in Fig. 4. The wavenumbers and widths of the transverse and longitudinal infrared branches can be then obtained, as summarized in Tables 2 and 3. To further confirm the fitting results of infrared spectra, the real and imaginary parts of $\epsilon(\omega)$ together with the imaginary part of ϵ^{-1} were calculated independently by using Kramers-Krönig (K-K) relation [30]. This is because the peak frequencies of the imaginary part of ϵ and ϵ^{-1}

Table 2

Dispersion parameters obtained from the best-fit by the 4-P model of infrared reflectivity spectra of the M-phase LaTiNbO₆ ceramics with A/B-site substitution (frequency and damping are in cm⁻¹).

j	M			M-A			M-B		
	$\Omega_{j,TO}/\gamma_{j,TO}$	$\Omega_{j,LO}/\gamma_{j,LO}$	$\Delta\epsilon_j$	$\Omega_{j,TO}/\gamma_{j,TO}$	$\Omega_{j,LO}/\gamma_{j,LO}$	$\Delta\epsilon_j$	$\Omega_{j,TO}/\gamma_{j,TO}$	$\Omega_{j,LO}/\gamma_{j,LO}$	$\Delta\epsilon_j$
1	118.6/13	125.5/17	4.29	119.9/10	122.5/10	1.99	122.6/12	123.5/12	0.56
2	134.5/17	142.0/24	1.85	133.3/35	147.1/17	4.51	141.9/24	144.2/18	2.05
3	154.9/13	157.3/19	0.54	156.0/18	161.0/16	0.90	154.4/49	192.2/73	6.59
4	172.2/33	179.8/27	1.35	167.0/22	180.0/19	0.91	206.3/32	211.6/54	0.26
5	214.0/20	217.6/18	0.72	210.0/27	216.0/23	0.70	231.0/15	232.1/18	0.09
6	235.0/15	238.0/14	0.56	232.0/22	237.0/19	0.51	261.8/42	275.6/49	1.30
7	264.8/34	270.7/32	1.50	264.0/40	270.0/25	1.25	286.5/29	295.1/42	0.35
8	285.8/33	305.9/32	2.37	276.0/35	298.0/38	0.98	317.1/51	333.5/97	0.59
9	321.1/42	336.7/55	0.84	318.0/54	339.0/59	0.69	376.6/64	383.6/97	0.29
10	388.4/71	415.5/60	2.51	383.0/93	416.0/72	1.19	451.1/109	468.8/95	1.07
11	431.5/63	469.7/75	1.09	436.0/77	472.0/75	0.47	484.8/101	500.6/137	0.41
12	484.7/70	517.2/117	0.46	487.0/76	503.0/114	0.11	554.3/228	642.7/63	1.64
13	549.8/131	635.0/62	0.86	568.0/172	630.0/96	0.72	653.6/59	742.1/82	0.12
14	648.0/55	738.8/72	0.12	657.0/91	733.0/98	0.20	780.3/41	796.7/42	0.03
15	770.2/43	792.8/49	0.03	773.0/69	799.0/78	0.04			
	$\epsilon_\infty = 4.19$			$\epsilon_\infty = 3.16$			$\epsilon_\infty = 3.99$		

Table 3

Dispersion parameters obtained from the best-fit by the 4-P model of infrared reflectivity spectra of the O-phase LaTiNbO₆ ceramics with A/B-site substitution (frequency and damping are in cm⁻¹).

j	O			O-A			O-B		
	$\Omega_{j,TO}/\gamma_{j,TO}$	$\Omega_{j,LO}/\gamma_{j,LO}$	$\Delta\epsilon_j$	$\Omega_{j,TO}/\gamma_{j,TO}$	$\Omega_{j,LO}/\gamma_{j,LO}$	$\Delta\epsilon_j$	$\Omega_{j,TO}/\gamma_{j,TO}$	$\Omega_{j,LO}/\gamma_{j,LO}$	$\Delta\epsilon_j$
1	98.0/8	102.4/8	7.84	99.5/13	102.6/11	5.68	99.0/12	101.0/11	3.24
2	136.6/24	149.7/14	20.2	110.1/54	113.5/68	3.46	143.0/32	150.0/25	10.5
3	152.1/11	157.9/18	1.27	144.6/31	152.6/19	8.54	179.0/41	212.0/27	24.2
4	178.2/8	195.1/13	13.3	185.2/31	218.0/25	18.7	219.0/32	234.0/28	2.40
5	195.2/11	213.2/11	0.05	225.3/27	237.8/23	1.68	242.0/34	256.0/41	1.88
6	219.0/14	234.7/25	1.19	248.1/28	261.8/32	1.86	267.0/49	289.0/45	2.24
7	256.6/30	295.5/29	4.31	273.7/32	293.1/32	1.83	315.0/70	366.0/41	4.63
8	296.1/32	302.2/36	0.03	323.9/43	363.7/47	4.06	376.0/47	440.0/49	1.02
9	320.3/22	360.1/50	1.74	387.8/54	446.4/52	2.46	455.0/50	502.0/58	0.52
10	385.0/37	445.0/42	1.68	458.6/53	509.0/77	0.58	533.0/70	558.0/75	0.62
11	453.8/36	510.8/89	0.29	544.6/98	633.4/186	1.11	574.0/91	705.0/77	0.56
12	550.8/69	626.7/235	0.64	637.4/139	709.7/72	0.06	728.5/133	792.0/42	0.11
13	652.8/135	701.6/54	0.19	733.4/103	803.5/65	0.11	824.1/57	841.9/34	0.03
14	730.0/71	795.4/68	0.13	829.6/61	842.8/72	0.02			
15	847.8/28	852.9/20	0.01						
	$\epsilon_\infty = 4.66$			$\epsilon_\infty = 5.22$			$\epsilon_\infty = 5.17$		

correspond to the values of transverse and longitudinal optical mode frequencies, respectively [15]. As shown in Fig. 5 using M and O-phase samples as representatives, all peaks for these two samples keep good agreements, indicating that the model is valid and the fitting results are reliable.

In addition, the oscillator strengths of the individual *j*th transverse optical modes can be obtained by using [15,27,28]

$$\Delta\epsilon_j = \frac{\epsilon_\infty}{\Omega_{j,TO}^2} \times \frac{\prod_k (\Omega_{k,LO}^2 - \Omega_{j,TO}^2)}{\prod_{k \neq j} (\Omega_{k,TO}^2 - \Omega_{j,TO}^2)} \quad (5)$$

The static (infrared) dielectric constant ϵ_0 , which corresponds to the intrinsic microwave dielectric constant, can be then obtained by adding the oscillator strengths of all modes as follows [15,27,28]:

$$\epsilon_0 = \epsilon_\infty + \sum_{j=1}^N \Delta\epsilon_j \quad (6)$$

Besides, the dielectric loss tangent (tan δ) can be given by adding the individual loss together as follows [28]:

$$\tan \delta = \sum_j \tan \delta_j = \sum_j \frac{\omega \Delta\epsilon_j \gamma_{j,TO}}{\epsilon_0 \Omega_{j,TO}^2} \quad (7)$$

The intrinsic (microwave-extrapolated) unloaded quality factor *Qu* can be then estimated using the reciprocal of the dielectric loss tangent. The final calculated values of ϵ_0 and *Qu* × *f* (at 10 GHz) are summarized in Table 4, together with microwave dielectric properties and related structure parameters of all studied LaTiNbO₆.

4. Discussion

In order to eliminate the influence of density, the measured permittivity ϵ_r has been corrected by porosity using the following equation [31]:

$$\epsilon_r = \epsilon_{rc} \left(1 - \frac{3P(\epsilon_{rc} - 1)}{2\epsilon_{rc} + 1} \right) \quad (8)$$

where ϵ_{rc} is the corrected dielectric constant and *P* is the fractional porosity of the compounds.

The intrinsic dielectric constant ϵ_0 calculated from the infrared spectra is found to be close to the ϵ_{rc} value (shown in Table 4), suggesting that the dielectric constant of the currently studied materials is mainly attributed to the dielectric response of intrinsic phonon. As found in in Table 3, the first six stronger modes at 98, 136.6, 178.2, 256.6, 320.3 and 385 cm⁻¹ for the O sample have together contributed

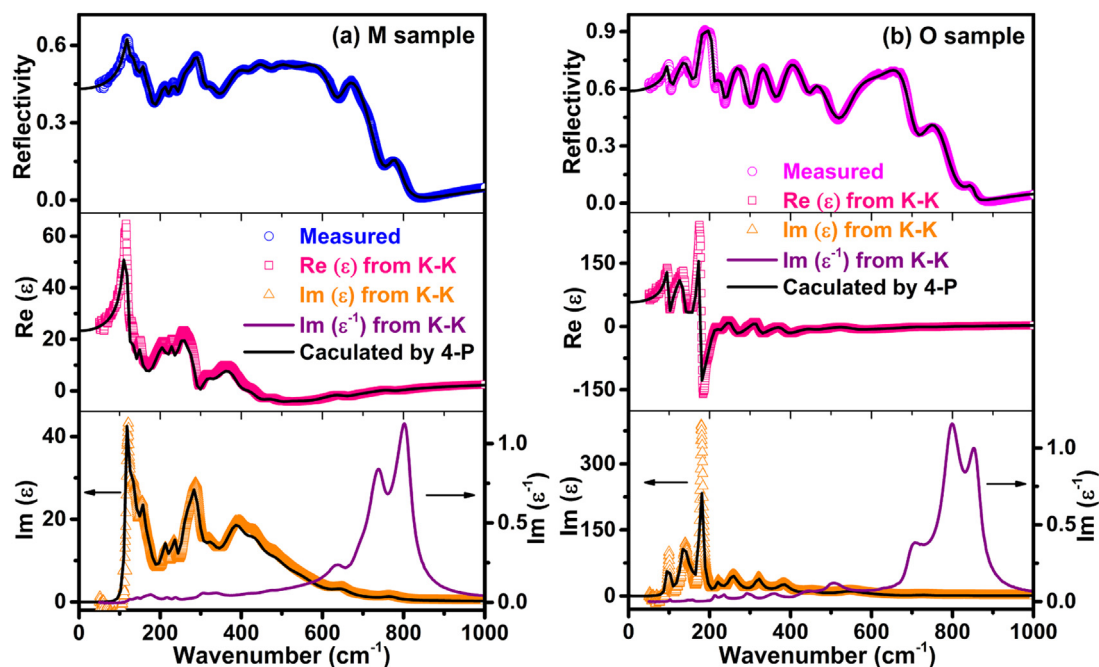


Fig. 5. Measured and adjusted infrared reflectivity spectra for the (a) M and (b) O samples, together with the real parts ($\text{Re}(\epsilon)$) of the complex dielectric function, and the imaginary parts of the direct ($\text{Im}(\epsilon)$) and reciprocal ($\text{Im}(\epsilon^{-1})$) dielectric functions, obtained from K-K analysis and 4-P model as indicated.

Table 4

Porosity and microwave dielectric properties and of A/B-site substituted LaTiNbO_6 ceramics with O and M-phase structures.

Porosity and dielectric properties	M phase			O phase		
	M	M-A	M-B	O	O-A	O-B
$P(\%)$	6.6	15.9	3.5	9.9	1.7	0.8
ϵ_r	22.5	15.9	21.0	48.7	52.6	56.2
ϵ_{rc}	24.8	20.5	22.1	56.9	53.9	56.9
$Q \times f$ (GHz)	68258	45154	96978	10018	15101	7382
f (GHz)	7.49	8.26	7.63	5.21	5.09	4.88
τ_f (ppm/°C)	-54	-53.8	-64.1	69.7	86.9	85.4
ϵ_0	23.3	18.3	19.3	57.6	55.4	57.1
$Q_u \times f$ (GHz)	58300	35900	29200	44100	28800	28700
Ref.	9	11	12	9	11	12

Ref.: The references for experimental values, i.e. P , ϵ_r , $Q \times f$, f , and τ_f in all six samples.

almost 85% of ϵ_0 . By comparison, 60% of ϵ_0 originates from the first six stronger modes at 118.6, 134.5, 172.2, 264.8, 285.8 and 388.4 cm^{-1} for the M sample in Table 2. Particularly, the first three vibration modes below 200 cm^{-1} for all six samples (O and M phases) give the majority of the dielectric contribution, corresponding to the external bending and stretching vibrations of the A-BO_6 [32]. By contrast, the dielectric contribution from the above remaining three strong vibration modes of 256.6, 320.3 and 385 cm^{-1} for the O sample in Table 3 is relatively small, and the slightly small dielectric contribution is also found in the vibration modes of 264.8, 285.8 and 388.4 cm^{-1} for the M sample in Table 2. These modes mainly originate from the bending and tilting vibration of BO_6 according to the mode assignment in Raman results (Fig. 2 and Table 1). Bond polarization might be the primary reason why dielectric contributions from the vibration of BO_6 differ from that of AO_8 [33]. Therefore, A–O bonds or the distortion of AO_8 polyhedra might have a great impact on the dispersion parameters of these three modes and consequently affect polarizabilities and intrinsic dielectric loss of LaTiNbO_6 , similar to the SrRAIO_4 (R = Sm, Nd, La) system [33]. That is to say, the big difference in ϵ_r values of M and O-phase LaTiNbO_6 ceramics (Table 4) should be primarily related with the

difference of their AO_8 structure units. There was no obvious change in the bond angle of AO_8 structure among current samples (This was not listed here). Moreover, considering that the bond angle has no direct relationship with polarizability, the A–O bond length was chosen for a further discussion. For clearer statements, the A–O bond length ($d_{\text{A-O}}$) of six different samples was then normalized by calculating the ratio of the actual bond length to the ideal one given by the sum of the effective ionic radii, as shown in Fig. 6. The actual bond length was obtained from the XRD Rietveld refinement results of our previous work [9,11,12]. It can be seen from Fig. 6 that the distribution of normalized $d_{\text{A-O}}$ is relatively dispersive in the M-phase samples, but it is relatively concentrated around 1 for the O-phase samples, clearly indicating a larger distortion of the AO_8 polyhedron in the M-phase. Besides, greatly compressed interlayer bonds of A–O3 and A–O4 in A-BO_6 were also observed in O-A sample of Fig. 6(b), which might be one of the reasons for its decreased permittivity. That is, when the bond length decreases, the binding force between electron and nucleus on the chemical bond would be strengthened, resulting in a decreased polarizability, and vice versa [34]. A similar change also existed in M phase though it is not obvious. Therefore, the substitution for A and B ions of M or O phase might change matrix ϵ_r through affect the A–O bonds associated with intrinsic A-BO_6 external vibration.

Compared with the measured quality factor $Q \times f$, the intrinsic $Q_u \times f$ calculated from the infrared spectra is relatively small in the M-phase structure, but relatively large in the O-phase structure (as shown in Table 4), although $Q_u \times f$ and $Q \times f$ are almost equivalent in theory. Nevertheless, all these quality factors are in the same order of magnitude. The deviation of $Q \times f$ might be mainly because the quality factor is more sensitive to defects than the permittivity. The inevitable defects on the polished sample surface would cause the light scattering, eventually leading to lost and fuzzy signals. A previous study [35] has also shown that the calculation of infrared reflectance spectroscopy can only give a rough estimation of the magnitude of intrinsic loss because of existing numerous influence factors. Therefore, a more accurate analysis might resort to the Terahertz spectroscopy in the future work.

It is interesting to note in Table 4 that an opposite sign of τ_f values was found in the M-phase and O-phase LaTiNbO_6 ceramics. The τ_f values are usually influenced by the structure-chemical characteristics of

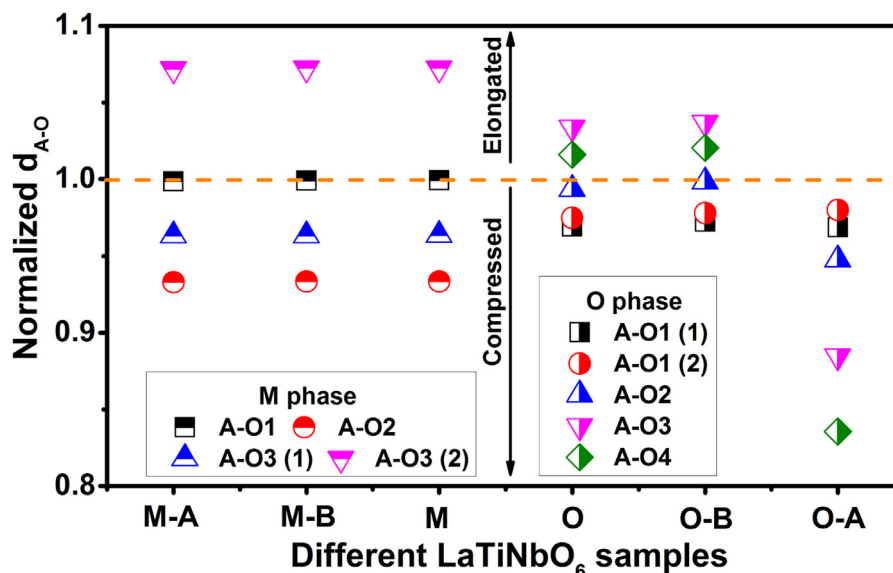


Fig. 6. Normalized d_{A-O} values in LaTiNbO_6 ceramics with different crystal structures.

dielectric oxides, especially the tilting of BO_6 octahedra [36]. It has been proposed that the octahedron in the O-phase sample with corner-sharing double-octahedron units should be more likely to tilt than that in the M-phase sample with edge-sharing double-octahedron units [12]. The Raman modes corresponding to the BO_6 tilting were found to be located in the frequency range of $340\text{--}520\text{ cm}^{-1}$, as seen from Fig. 2. These modes in the O-phase sample appear at lower wavenumbers than that in the M-phase sample, indicating that the octahedron in the O-phase structure is more prone to tilt basically as a result of their different octahedral connection ways. This is similar to the case in the complex perovskite structure [37], where τ_f would change its sign as a phase transition occurs from a non-tilting cubic structure to a tilting structure with a lower symmetry.

5. Conclusions

Raman scattering and infrared reflection spectra of the M and O-phase LaTiNbO_6 ceramics by A/B-site substitution were studied with the help of Lorentz fitting, 4-P model and K-K equation for the purpose to disclose the relation between the local structure and microwave dielectric properties. Compared with Raman spectra of the M phase, the stretching vibration of B–O–B and O–B–O bonds at 659 cm^{-1} was only found in the special interlayer chain structure of O phase. Results of infrared spectra reveal that the dielectric response of M and O phases mainly originates from the A- BO_6 external vibrations in the far-infrared frequency. The dielectric constant should be mainly attributed to the dielectric response of intrinsic phonon in current work, leading to different ϵ_r values between M and O phases as a result of their AO_8 structure unit, especially the relevant A–O bonds. However, the sign-opposite τ_f values observed in M and O-phase LaTiNbO_6 ceramics structures are attributed to their different octahedron connection ways, which should correspond to the Raman mode of the BO_6 tilting vibration within $340\text{--}520\text{ cm}^{-1}$. These results would be helpful for a better understanding the structure-property relation in typical $\text{RETi}(\text{Nb,Ta})\text{O}_6$ microwave dielectric materials.

Acknowledgements

This work was financially supported by the National Natural Science Foundation of China (Grant No. 51272060).

References

- [1] X. Qi, T.P.J. Han, H.G. Gallagher, B. Henderson, R. Illingworth, I.S. Ruddle, Optical spectroscopy of PrTiNbO_6 , NdTiNbO_6 and ErTiNbO_6 single crystals, *J. Phys. Condens. Matter* 8 (1996) 4837–4845.
- [2] X. Qi, R. Illingworth, H.G. Gallenger, T.P.J. Han, B. Henderson, Potential laser gain media with the stoichiometric formula RETiNbO_6 , *J. Cryst. Growth* 160 (1996) 111–118.
- [3] X. Qi, C.M. Liu, C.C. Kuo, Pr^{3+} doped LaTiNbO_6 as a single phosphor for white LEDs, *J. Alloy. Compd.* 492 (2010) L61–L63.
- [4] M.T. Sebastian, S. Solomon, R. Ratheesh, J. George, P. Mohanan, Preparation, characterization, and microwave properties of RETiNbO_6 (RE = Ce, Pr, Nd, Sm, Eu, Gd, Tb, Dy, Y, and Yb) dielectric ceramics, *J. Am. Ceram. Soc.* 84 (2001) 1487–1489.
- [5] K.P. Surendran, S. Solomon, M.R. Varma, P. Mohanan, M.T. Sebastian, Microwave dielectric properties of RETiTaO_6 (RE = La, Ce, Pr, Nd, Sm, Eu, Gd, Tb, Dy, Ho, Y, Er, Yb, Al, and In) ceramics, *J. Mater. Res.* 17 (2002) 2561–2566.
- [6] K.P. Surendran, M.R. Varma, P. Mohanan, M.T. Sebastian, Microwave dielectric properties of $\text{RE}_{1-x}\text{RE}'_x\text{TiNbO}_6$ [RE = Pr, Nd, Sm; RE' = Gd, Dy, Y] ceramics, *J. Am. Ceram. Soc.* 86 (2003) 1695–1699.
- [7] V.I. Strakhov, O.V. Mel'nikova, M. Dib, Phase diagram for the system $\text{LaNbO}_4\text{--TiO}_2$, *Inorg. Mater.* 27 (1991) 495–498.
- [8] J.J. Bian, Y.Z. Li, L.L. Yuan, Structural stability and microwave dielectric properties of $(1-x)\text{Ln}_{1/3}\text{NbO}_3\text{--}x\text{Ln}_{2/3}\text{TiO}_3$ (Ln: La, Nd; $0 \leq x \leq 0.8$), *Mater. Chem. Phys.* 116 (2009) 102–106.
- [9] J. Zhang, R.Z. Zuo, A novel self-composite property-tunable LaTiNbO_6 microwave dielectric ceramic, *Mater. Res. Bull.* 83 (2016) 568–572.
- [10] J. Zhang, R.Z. Zuo, Sintering behavior, structural phase transition and microwave dielectric properties of $\text{La}_{1-x}\text{Zn}_x\text{TiNbO}_{6-x/2}$ ceramics, *J. Am. Ceram. Soc.* 100 (2017) 4362–4368.
- [11] J. Zhang, R.Z. Zuo, Phase structural transition and microwave dielectric properties in isovalently substituted $\text{La}_{1-x}\text{Ln}_x\text{TiNbO}_6$ (Ln=Ce, Sm) ceramics, *Ceram. Int.* 43 (2017) 7065–7072.
- [12] J. Zhang, R.Z. Zuo, Octahedral distortion, phase structural stability and microwave dielectric properties in equivalently substituted LaTiNbO_6 ceramics, *J. Am. Ceram. Soc.* 100 (2017) 5249–5258.
- [13] L.X. Pang, D. Zhou, Z.M. Qi, W.G. Liu, Z.X. Yue, I.M. Reaney, Structure–property relationships of low sintering temperature scheelite-structured $(1-x)\text{BiVO}_4\text{--}x\text{LaNbO}_4$ microwave dielectric ceramics, *J. Mater. Chem. C* 5 (2017) 2695–2701.
- [14] W.B. Li, D. Zhou, L.X. Pang, G.H. Chen, Z.M. Qi, Q.P. Wang, H.C. Liu, Structure, Raman spectra, far-infrared spectra and microwave dielectric properties of temperature independent $\text{CeVO}_4\text{--TiO}_2$ composite ceramics, *J. Alloy. Compd.* 694 (2017) 40–45.
- [15] K.P.F. Siqueira, R.L. Moreira, A. Dias, Synthesis and crystal structure of lanthanide orthoniobates studied by vibrational spectroscopy, *Chem. Mater.* 22 (2010) 2668–2674.
- [16] A. Dias, G. Subodh, M.T. Sebastian, M.M. Lage, R.L. Moreira, Vibrational studies and microwave dielectric properties of A-site-substituted tellurium-based double perovskites, *Chem. Mater.* 20 (2008) 4347–4355.
- [17] A. Dias, F.M. Matinaga, R.L. Moreira, Raman spectroscopy of $(\text{Ba}_{1-x}\text{Sr}_x)(\text{Mg}_{1/3}\text{Nb}_{2/3})\text{O}_3$ solid solutions from microwave-hydrothermal powders, *Chem. Mater.* 19 (2007) 2335–2341.
- [18] A. Golobič, S.D. Škapin, D. Suvorov, A. Meden, Solving structural problems of ceramic materials, *Croat. Chem. Acta* 77 (2004) 435–446.
- [19] E. Kroumova, M.I. Aroyo, J.M. Perez-Mato, A. Kirov, C. Capillas, S. Ivantchev,

- H. Wondratschek, Bilbao crystallographic server: useful databases and tools for phase-transition studies, *Phase Transit.* 76 (2003) 155–170.
- [20] M. Kasunič, S.D. Škapin, D. Suvorov, A. Golobič, Polymorphism of LaTaTiO_6 , *Acta Chim. Slov.* 59 (2012) 117–123.
- [21] C.W.A. Paschoal, R.L. Moreira, C. Fantini, M.A. Pimenta, K.P. Surendran, M.T. Sebastian, Raman scattering study of RETiTaO_6 dielectric ceramics, *J. Eur. Ceram. Soc.* 23 (2003) 2661–2666.
- [22] R.L. Moreira, J.I. Viegas, A. Dias, Raman and infrared spectroscopic studies of LaTaTiO_6 polymorphs, *J. Alloy. Compd.* 710 (2017) 608–615.
- [23] L. Xue, W. Gong, A study on Raman and photoluminescence spectra of the aeschynite group minerals, *Spectrosc. Spect. Anal.* 20 (2000) 827–829.
- [24] Y. Repelin, E. Husson, N.Q. Dao, H. Brusset, Etude par spectroscopies d'absorption ir et de diffusion Raman des composés $\text{A}^{\text{III}}\text{B}_2^{\text{VI}}\text{O}_6$ de structure de type "blocs 1×2 "—II. Etude du niobate de strontium SrNb_2O_6 et des tantalates de calcium CaTa_2O_6 et de baryum BaTa_2O_6 (II), *Spectrochim. Acta A* 35 (1979) 1165–1175.
- [25] Q. Liao, L. Li, Structural dependence of microwave dielectric properties of ixiolite structured $\text{ZnTiNb}_2\text{O}_8$ materials: crystal structure refinement and Raman spectra study, *Dalton Trans.* 41 (2012) 6963–6969.
- [26] F. Gervais, P. Echegut, *Incommensurate phases in dielectrics*, North Holland, Amsterdam, 1986.
- [27] R.L. Moreira, A. Feteira, A. Dias, Raman and infrared spectroscopic investigations on the crystal structure and phonon modes of LaYbO_3 ceramics, *J. Phys. Condens. Matter* 17 (2005) 2775–2781.
- [28] N.G. Teixeira, R.L. Moreira, R.P.S.M. Lobo, M.R.B. Andreetta, A.C. Hernandes, A. Dias, Raman and infrared phonon features in a designed cubic polymorph of CaTa_2O_6 , *Cryst. Growth Des.* 11 (2011) 5567–5573.
- [29] D.D.S. Meneses, G. Gruener, M. Malki, P. Echegut, Causal voigt profile for modeling reflectivity spectra of glasses, *J. Non-Cryst. Solids* 351 (2005) 124–129.
- [30] W. Hayes, R. Loudon, *Scattering of Light by Crystals*, Wiley, New York, 1978.
- [31] S.J. Penn, N.M. Alford, A. Templeton, X. Wang, M. Xu, M. Reece, K. Schrapel, Effect of porosity and grain size on the microwave dielectric properties of sintered alumina, *J. Am. Ceram. Soc.* 80 (1997) 1885–1888.
- [32] C.W.A. Paschoal, R.L. Moreira, K.P. Surendran, M.T. Sebastian, Infrared reflectivity and intrinsic dielectric behavior of RETiTaO_6 (RE = Y, Ce, Pr, Nd, Sm, Eu, Gd, Tb, Dy, Ho, Er, and Yb) microwave ceramics, *J. Mater. Res.* 20 (2005) 1164–1171.
- [33] X.C. Fan, X.M. Chen, X.Q. Liu, Structural dependence of microwave dielectric properties of SrRAIO_4 (R=Sm, Nd, La) ceramics: crystal structure refinement and infrared reflectivity study, *Chem. Mater.* 20 (2008) 4092–4098.
- [34] Z. Liu, G. Wu, Asymmetric environment around the thiourea molecule in aqueous solution as evidenced by the bond polarizability derivatives from Raman intensity, *Chem. Phys.* 316 (2005) 25–28.
- [35] J. Petzelt, S. Kamba, Submillimetre and infrared response of microwave materials: extrapolation to microwave properties, *Mater. Chem. Phys.* 79 (2003) 175–180.
- [36] E.L. Colla, I.M. Reaney, N. Setter, A microscopic model for the temperature coefficient of the resonant frequency (τ_f) in complex perovskites used for microwave filter, *Ferroelectrics* 154 (1994) 35–40.
- [37] M.P. Seabra, V.M. Ferreira, H. Zheng, I.M. Reaney, Structure property relations in $\text{La}(\text{Mg}_{1/2}\text{Ti}_{1/2})\text{O}_3$ -based solid solutions, *J. Appl. Phys.* 97 (2005) 033525.